JTTEE5 18:256–271
DOI: 10.1007/s11666-009-9300-y
1059-9630/$19.00 © ASM International

Arc Sprayed Steel: Microstructure in Severe Substrate Features

A.P. Newbery and P.S. Grant

(Submitted August 16, 2008; in revised form January 6, 2009)

The effect of severe substrate topography on the microstructure of thermally sprayed coatings has been relatively neglected, but is critical in controlling the performance of thick electric arc sprayed steel shells for rapid tooling applications. This paper shows how the spray angle and the atomizing gas pressure control the distribution of porosity and oxide in steel sprayed in and around cylindrical holes of different diameter and depth. Droplet splashing and the secondary deposition of splash droplets caused systematic variations in microstructure. In particular, the origin of the phenomenon of "bridging," the premature closure of features, has been revealed by microstructural analysis and explained in terms of the trajectories of droplets. The filling of features with higher-quality material can be aided by using a low atomizing gas pressure, reducing the oxygen partial pressure of the surrounding atmosphere and careful selection of the spray angle.

Keywords droplet splashing, oxide, porosity, rapid tooling, spray parameters, twin wire electric arc

1. Introduction

Twin wire electric arc (Ref 1), a relatively inexpensive and easy-to-use thermal spray technique, is used to form a variety of coatings for anticorrosion, wear resistance, and dimensional restoration. Arc spraying creates a molten droplet spray by forming a direct current (DC) arc between two consumable conductive wires, as shown schematically in Fig. 1. The high temperature of the arc melts the wire tips; a gas flow atomizes this molten material and then propels the resulting droplets toward the substrate to be coated. The liquid droplets spread on impact, and a coating is built up by the addition of successive "splats." In common with other thermal spraying techniques, rapid solidification during droplet spreading not only prevents complete fusion with the previous splats, but also prevents the complete filling of interstices in the structure (Ref 2), leading to characteristic microporosity. Although an arc sprayed coating is predominantly composed of lamellar splats, the structure usually contains spherical presolidified droplets (PSDs), droplets that have solidified in flight, prior to deposition. Typically, air is used as the atomizing gas and in-flight oxidation leads to intersplat oxide and further undermining of the coating coherence. The bulk properties are thus determined by the properties of the splat interfaces, in addition to the properties of the sprayed material itself.

A.P. Newbery and **P.S. Grant**, Department of Materials, University of Oxford, Oxford, UK. Contact e-mails: piersn@hotmail.com, Patrick.grant@materials.ox.ac.uk.

Although mostly a coating process, where the deposits are less than 1 mm thick, arc spraying has been employed to lay down zinc, aluminum, or other soft materials to a greater thickness on a dimensionally accurate pattern. The resulting shell is removed from the pattern, trimmed, and backed to produce an insert suitable for tooling (Ref 3-12). Until recently, the manufacture of arc sprayed steel shells for production applications has been impossible because of excessive warping and distortion during spraying and subsequent cooling. However, by the control of temperature, thermal stresses, and phase transformations (Ref 13, 14), arc spraying has been demonstrated for the rapid manufacture of steel tooling for plastic injection molds and other applications. This technique involves the robotic manipulation of multiple arc guns over a sacrificial freeze-cast ceramic pattern and can substantially cut the lead time and cost compared with conventional tooling production methods (Ref 6, 15).

The replication of severe topographic features in the pattern/substrate is problematic. The two main difficulties encountered when spraying into a narrow channel, for example, as shown in Fig. 2, are: (a) the premature impingement, or joining, of the free surfaces of the deposit across the entrance of the feature, known as "bridging," that leads to the creation of a macropore and (b) the formation of thin, poor-quality material on the feature side walls (Ref 16, 17). The combination of these phenomena leads to a structurally weak deposit when the ceramic substrate is removed. If so, either a steel insert can be used (Ref 6), or the feature enlarged and then excess material conventionally machined after spraying. However, the need for such inserts or postspray machining reduces the time and cost advantage of the spraying process.

Splashing of the spray droplets on impact with the substrate or top surface of the growing deposit during arc spraying is endemic (Ref 17, 18). The subsequent behavior of the droplets generated by splashing influences the

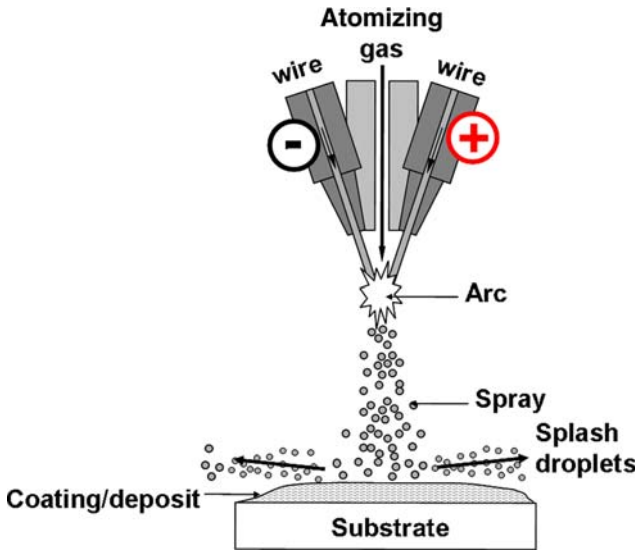

Fig. 1 Schematic diagram showing the twin wire electric arc spray process for the formation of coatings or free standing deposits

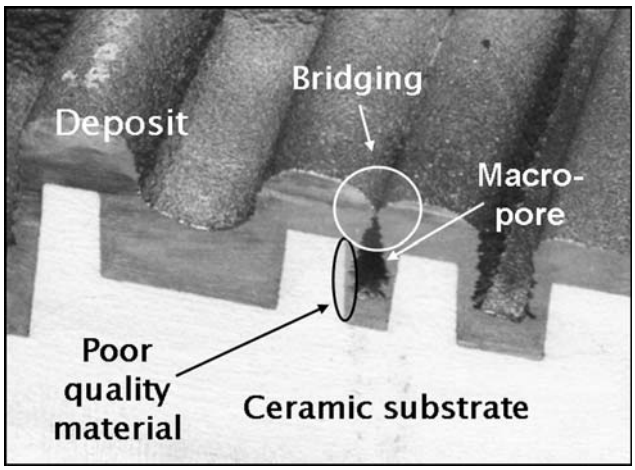

Fig. 2 Common problems when arc spraying into a narrow substrate feature, such as a channel. Bridging leads to the formation of a large macropore, and the deposit on the side wall is thin and of low quality

evolution of deposit shape and structure when conditions are such that their trajectory intersects the substrate (or deposit), rather than being carried away by the atomizing gas to form ''overspray'' (Ref 17, 19-22).

This paper presents an investigation of thick deposits formed by the arc spraying of steel onto a substrate containing severe topographical features. In particular, the effect of spray angle and atomizing gas pressure on the porosity and oxide in and around cylindrical holes of different diameters and depths is investigated. A number of explanations are proposed for the origin of various microscopic and macroscopic deposit structures.

2. Experimental Procedure

Two model experiments were carried out in order to characterize splashing behavior and splash droplets. This information was then used to understand the evolution of deposit shape and microstructure observed in experiments described in section 2.3. All experiments used a Sulzer-Metco SmartArc system (Sulzer Metco US Inc., Westbury, NY, USA) to spray 1.6 mm diameter Fe-0.8 wt.%C steel wire (TAFA 38T, TAFA Inc., Concord, NH, USA).

2.1 Effect of Atomizing Gas Pressure on Droplet Diameter

The arc gun was mounted on the top of a sealed chamber to exclude ambient air. A series of thin deposits were produced by spraying onto the center of a 350 × 230 mm static mild steel plate, sufficiently large that there was no overspray; that is, collected steel powder at the end of spraying could only have originated from droplet splashing or bounce-off. Prior to spraying, the plate was grit blasted with alumina and cleaned using methanol, and the chamber was purged with N_2 to remove air. The spraying conditions were: an arc voltage of 28 V, a wire feed rate of 1.14 g/s, an arc current of 95 A, a spray distance of 150 mm, and N_2 atomizing gas pressures in the range 140 to 450 kPa. A combination of low wire feed rate and voltage was chosen to avoid excessive deposit overheating and melting. The spray duration was 60 s. After spraying, each deposit was weighed, and all powder inside the chamber and extraction cyclone was collected, sieved, weighed, and its mass median diameter determined. For comparison, the mass median powder diameter of the primary spray (under identical arc conditions) was determined without a substrate using a 2.6 m chamber extension, which is sufficiently long for all the droplets to solidify before impact.

2.2 Secondary Deposition Profile

Using the sealed chamber described previously, the splash droplets from spraying onto a steel insert, shown in Fig. 3, were collected in the form of a deposit on a recessed vertical side wall, always in shadow from the primary spray. The purpose of these experiments was to measure the spatial distribution of mass associated with droplet splashing; that is, what was the range of trajectories taken by splash droplets emitted about a primary droplet impact on a flat surface. This information was then used to understand where splash droplets tended to redeposit in more complex geometries. The spray conditions were: an arc voltage of 35 V, a wire feed rate of 2.46 g/s, an arc current of 200 A, and a spray distance of 200 mm, typical for spraying rapid steel tooling. The chamber was purged with N_2 for 60 s before spraying, and the spray duration was 6 s. A series of experiments were carried out at atomizing gas pressures of 140 to 550 kPa, using either N_2 or air. The deposits formed on the side wall were weighed. One of the deposit profiles was determined by vertical sectioning through the maximum

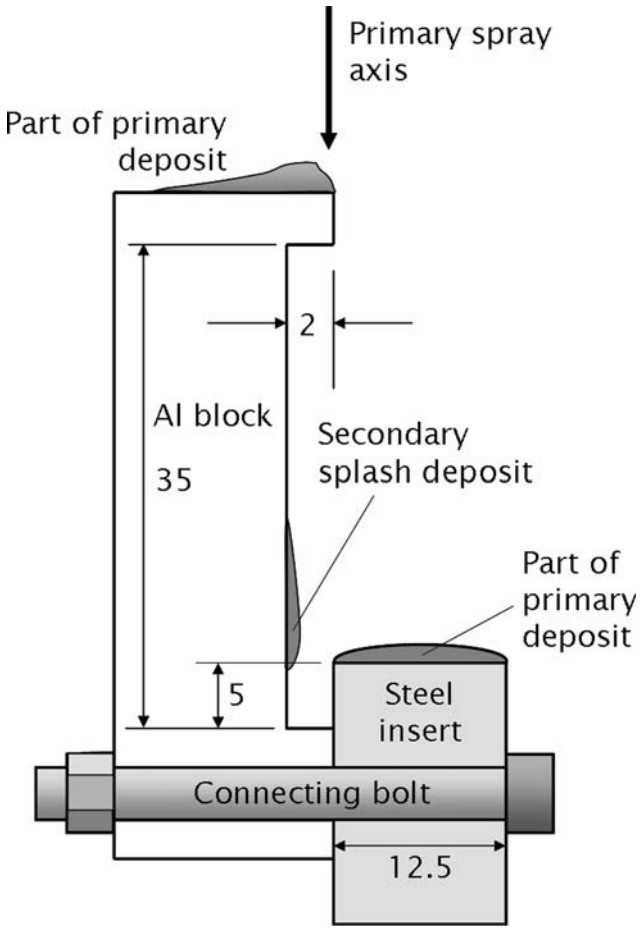

Fig. 3 Schematic diagram showing the arrangement for the secondary deposition of splash droplets generated by spraying onto a steel insert. All dimensions are in mm

thickness, mounting it, and then using an *x-y* table with a Vernier scale of accuracy 0.1 mm.

2.3 Spraying onto a Substrate Containing Holes

These experiments employed a setup used for spraying steel tooling in which the arc gun is mounted to the arm of a Motoman K60 industrial six-axis robot. The robot scanned the spray at a constant speed and distance (from the substrate surface), in a zig-zag manner, over a 200 by 150 by 50 mm alumina-based freeze-cast substrate placed on a large rotating table, so that a deposit of even thickness of ~17 mm, was formed over the flat surface. The spraying conditions are given in Table 1. Spraying took place enclosed in a booth that incorporated a roof-mounted extraction system to remove ''weld fume,'' the very fine dust generated by arc spraying. Although N_2 atomizing gas was used, the surrounding atmosphere was largely air, since ambient air was continually drawn in through the roof of the booth as a result of the large flow exerted by the extraction system.

The effect of three variables on the deposit structure was investigated:

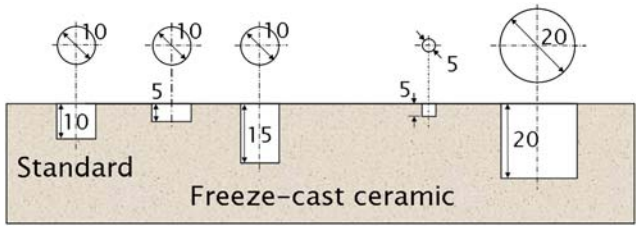

Fig. 4 Cross section of the ceramic substrate used to investigate the filling and microstructure of deposit formed by spraying into cylindrical holes

Table 1 Conditions for the robotic electric arc spraying of 0.8 wt.% C steel onto ceramic substrates containing cylindrical holes

Parameter	Value
Arc voltage, V	30
Wire feed rate, g/s	2.65
Arc current, A	230
Atomizing gas	Nitrogen
Atomizing gas pressure, kPa	140 or 450
Substrate table rotation, rpm	2
Gun traverse speed, m/s	0.11
Spray angle, degrees	90 or 45
Spray distance, mm	150
Spray duration, min	40

Spray angle. Defined as the angle between the spray axis and the flat top surface of the substrate; that is, 90° indicates spraying vertically downward onto the horizontal substrate. Two values were chosen, 45° and 90°. The spray angle was varied by altering the arc gun mounting on the robot and was constant throughout a particular experiment.

Atomizing gas pressure. Two pressures, 140 and 450 kPa, were used.

Hole diameter and depth. In addition to a central flat area, each substrate contained five flat-bottomed cylindrical holes of different dimensions: 10 by 10 mm (standard), 5 by 5 mm (small), 20 by 20 mm (large), 10 by 5 mm (shallow), and 10 by 15 mm (deep), as shown in Fig. 4. Holes were used to ensure axisymmetry of the features formed and represent typical pins or protrusions in the finished tool; ribs are also important features in a finished tool and would be formed by spraying into slots in the substrate, but break axis-symmetry. A 10 by 10 mm hole was chosen as standard because it typically represents the smallest feature that can be filled by sprayed material without excessive bridging and is thus well suited to test the efficacy of various processing approaches to enhance filling.

Steel deposits and ceramic substrates were sectioned using a diamond cutoff wheel. To prevent weak deposit regions from fracture, any macropores were filled with a cold mounting resin, prior to final removal of any residual

ceramic by grit blasting with cast iron shot. Samples were then cold mounted, ground, and polished using standard metallographic procedures for unetched examination by optical microscopy. Image analysis was used to quantify the area fraction of deposit oxide (gray) and porosity (black) in the steel (white). Deposit samples from the central, flat area of the substrate were sent to London & Scandinavian Metals, United Kingdom, for chemical analysis of oxygen.

3. Results

3.1 Effect of Atomizing Gas Pressure on Droplet Diameter

Increasing the gas pressure from 140 to 550 kPa decreased the mass median diameter of primary spray powder from 125 to 61 μm, as shown in Fig. 5, because of the more effective break-up of the molten metal at the wire tips and in flight (Ref 23). Likewise, the mass median diameter of the splash droplets from spraying also decreased, from 46 to 20 μm; that is, the splash droplets had a mass median diameter approximately one-third of the primary spray. At all atomizing gas pressures investigated, the deposition efficiency (deposited mass/sprayed mass) spraying onto a large plate was in the range 63 to 66%.

3.2 Secondary Deposit Profile

An example of the cross-sectional profile of a deposit formed entirely by splash droplets is shown in Fig. 6. The maximum splash deposit thickness was 1.3 mm and occurred ~1 mm above the horizontal surface of the primary substrate (the steel insert); that is, most splash droplets traveled close and parallel to the substrate prior to deposition. A significant proportion of deposit was formed below the level of the primary substrate, confirming previous observations of splash droplet behavior near a step (Ref 18). As shown later, this behavior is often significant in deposit formation when spraying around a severe substrate feature.

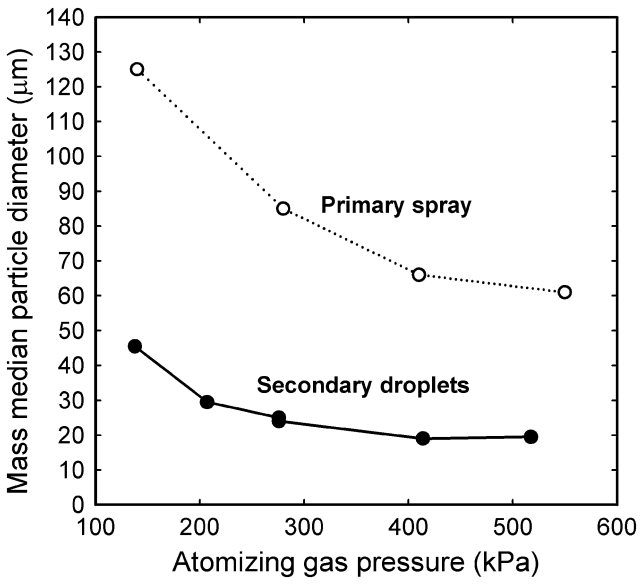

Fig. 5 The effect of atomizing gas pressure on the mass median particle diameter of powder generated by the primary spray without a substrate, and splashing of the primary spray depositing on to a large steel substrate (secondary droplets)

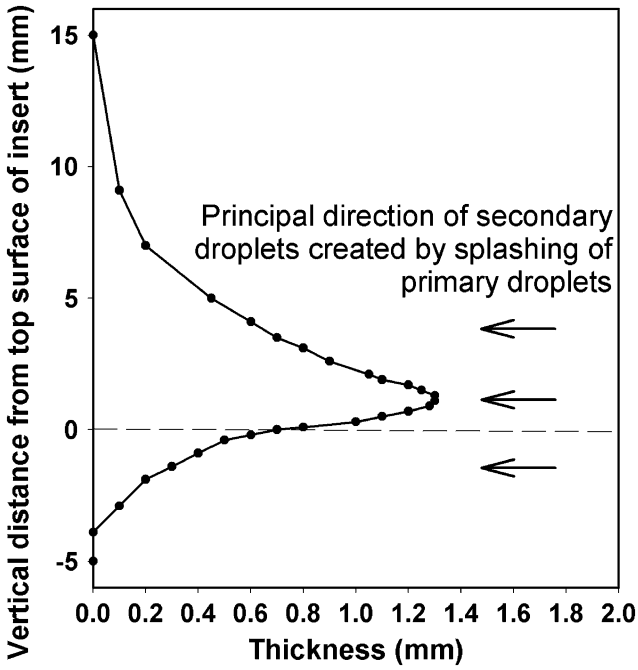

Fig. 6 The cross-sectional profile of a side-wall deposit formed by the secondary deposition of splash droplets, generated by spraying statically onto a nearby substrate (a steel insert, shown in Fig. 3)

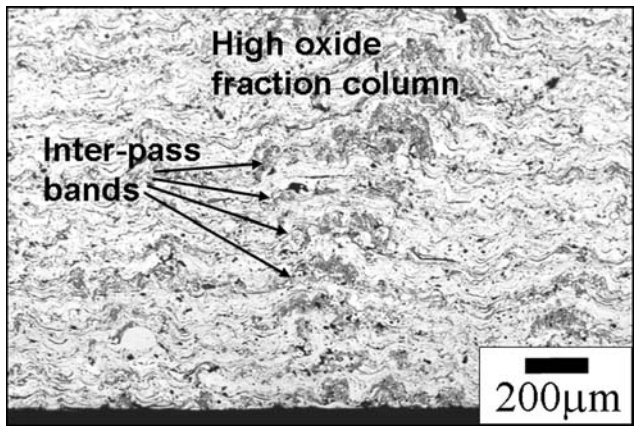

Fig. 7 Optical micrograph (unetched) near the substrate of a thick deposit formed by spraying onto the flat part of a freeze-cast ceramic at a angle of 90° and an atomizing gas pressure of 450 kPa. The steel, oxide, and pores appear white, gray, and black, respectively

For N_2 atomizing gas, the deposits formed from splash droplets were 20 to 27% of the total mass of the metal sprayed, whereas for air atomization, the mass fraction was 28 to 33% probably because of an increase in the oxidation of the splash droplets, although an increase in the amount of splashing caused by the exothermic heating of the droplets (and reduced viscosity) due to oxidation (Ref 24), and/or an increase in the splash deposition efficiency could also be factors. For both types of atomizing gas, the mass of the splash deposit increased with increasing atomizing gas pressure. Again, this was most likely because of an increase in the fraction of oxidation associated with the finer primary droplet diameters produced at higher pressures.

3.3 Deposit Structure on Flat Areas

For the deposits formed on flat area of substrate, away from the influence of a hole, the lamellar splat microstructure was largely typical of arc sprayed coatings, with oxide in the form of intersplat stringers, as shown for a deposit sprayed at 90° and 450 kPa in Fig. 7. The amount of oxide in this case was generally ~7%, while the porosity was in the range 3 to 6%. However, a significant structural feature of these thick deposits, not observed in thinner coatings, was the presence of vertical columns containing as much as 30% oxide, also shown in Fig. 7. These high oxide columns originated from perturbations, often near the substrate, and diverged outward as they moved upward through the deposit. The columns consisted of interpass oxide bands, containing high numbers of small diameter, presolidified splash droplets. Where the column reached the deposit top surface, a macroscopic ''dune'' resulted. When viewed in plan section near the deposit top surface, the columns were visible as rings of oxide, several millimeters in diameter.

The scale of the microstructure comprising splats, pores, and oxide became finer and surface dunes became

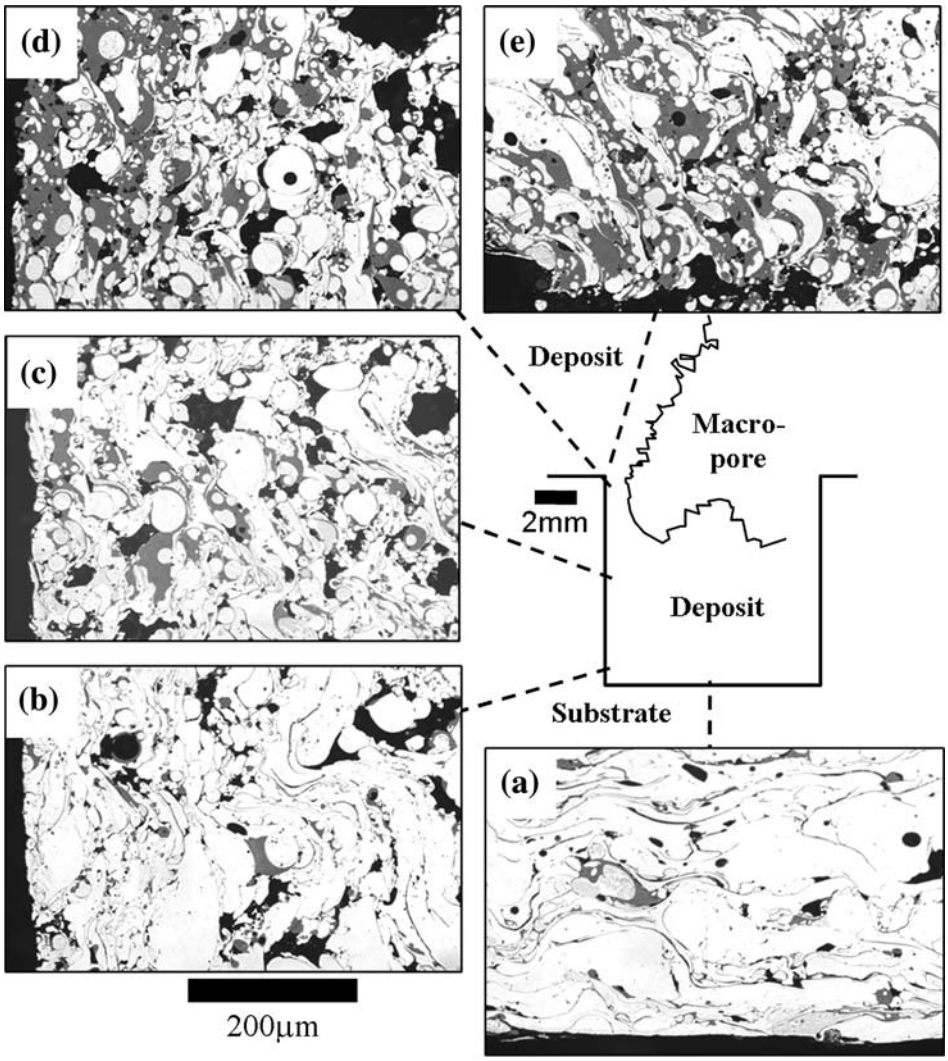

Fig. 8 Optical micrographs of different positions in a deposit formed by spraying into a 10 by 10 mm (standard) cylindrical hole, at an angle of 90° and an atomizing gas pressure of 140 kPa. (a) Hole base, (b) side wall near base corner, (c) side wall half-way up, (d) side wall near top corner, and (e) top corner

more pronounced as the atomizing gas pressure was increased. Increasing the atomizing gas pressure from 140 to 450 kPa also increased the amount of oxide and the oxygen concentration (measured by chemical analysis) from 1.6 to 3.2 wt.%. The oxygen concentration was also higher for deposits sprayed at an angle of 90° rather than those sprayed at 45°.

3.4 Deposit Structure in and Around Cylindrical Holes

3.4.1 Standard (10 by 10 mm) Hole. For the deposit sprayed at an angle of 90° and an atomizing gas pressure of 140 kPa, there were relatively low oxide fractions (~8%), porosity fractions (4-6%) and numbers of PSDs at the base of the 10 by 10 mm hole, as shown in Fig. 8(a). The microstructure in the base was similar to that of the deposit formed away from the hole (without the high oxide columns). At the side walls, the splats were smaller and there was higher porosity and numbers of PSDs, as shown in Fig. 8(b). Further up the side walls, the fraction of oxide and porosity increased: oxide from 9 to 22% and porosity from 10 to 23%, as shown in Fig. 8(c), (d), and (e), and in Fig. 9(a) and (b). For both oxide and porosity, the increase was most marked near the top of the hole where the deposit contained a comparatively high number of PSDs, with diameters in the range 5 to 70 μm. The smaller PSDs were typically associated with a large local fraction of oxide.

3.4.2 Spray Angle. All the deposits around the holes, except for the 10 by 5 mm (shallow) hole sprayed at an angle of 90°, contained single macropores on the hole axis. There were two types of macropore shape, shown schematically in Fig. 10, dependent on the spray angle:

Inverse heart. Obtained at a spray angle of 90°. The thinnest regions of the deposit occurred on the side walls, just below the top corner of the hole and were particularly susceptible to fracture.

Triangle. Obtained at a spray angle of 45°. The thinnest, most fragile regions of deposit occurred again on side walls, though near the base. The triangle walls were curved, tending toward a teardrop shape, most notably for the 10 by 5 mm (shallow) hole.

Typically, the upper surfaces of both shapes were rough and jagged, a characteristic structural feature that has been observed previously (Ref 17).

The deposit at the base of the 10 by 10 mm hole formed by spraying at an angle of 45°, compared with that sprayed at 90°, contained relatively high oxide (~10%) and porosity (5-13%) fractions, and a high fraction of PSDs, as shown in Fig. 11(a). At the side wall, the microstructure was coarser, as shown in Fig. 11(b) and (c). Approximately 2 mm from the hole base, the side wall deposit contained pores that were large, elongated, and arranged in lines, which fanned upwards and away from the side wall at angles between 90 and 45°, increasing the local porosity fraction to ~30%, as shown in Fig. 12. Some of the elongated pores connected from the side wall to the central macropore. Further up the side wall, the size of these large pores progressively decreased and the local

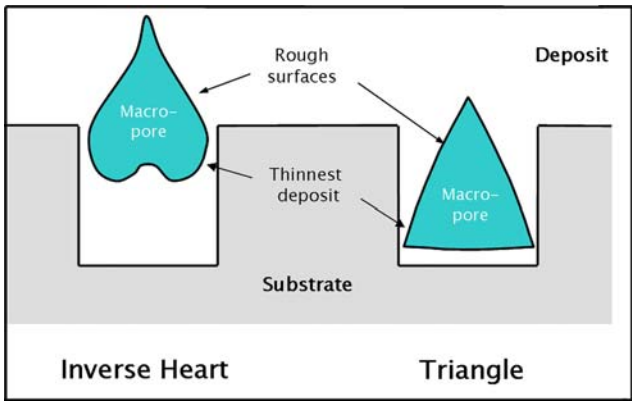

Fig. 10 Schematic diagram showing the two main types of macropore shape obtained in deposits formed by spraying onto a substrate containing cylindrical holes

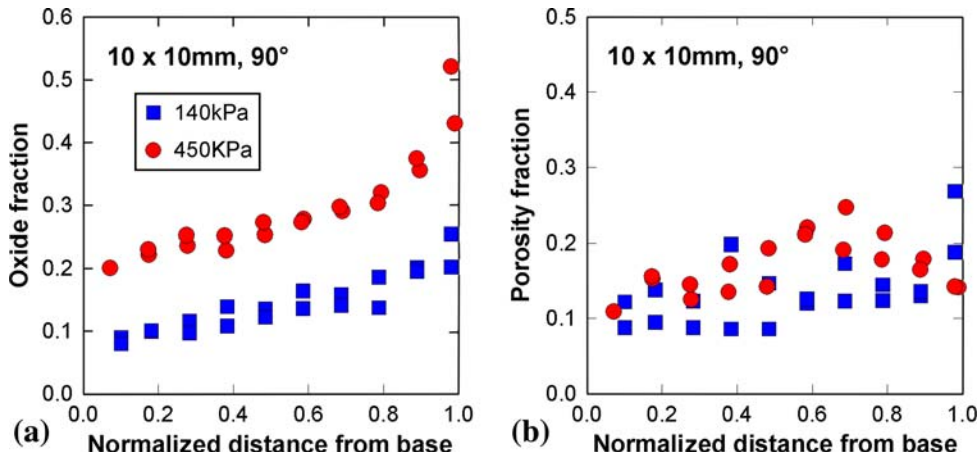

Fig. 9 Variation of (a) oxide and (b) porosity up the side walls of deposits formed by spraying into 10 by 10 mm (standard) cylindrical holes at an angle of 90° at atomizing gas pressures of 140 and 450 kPa

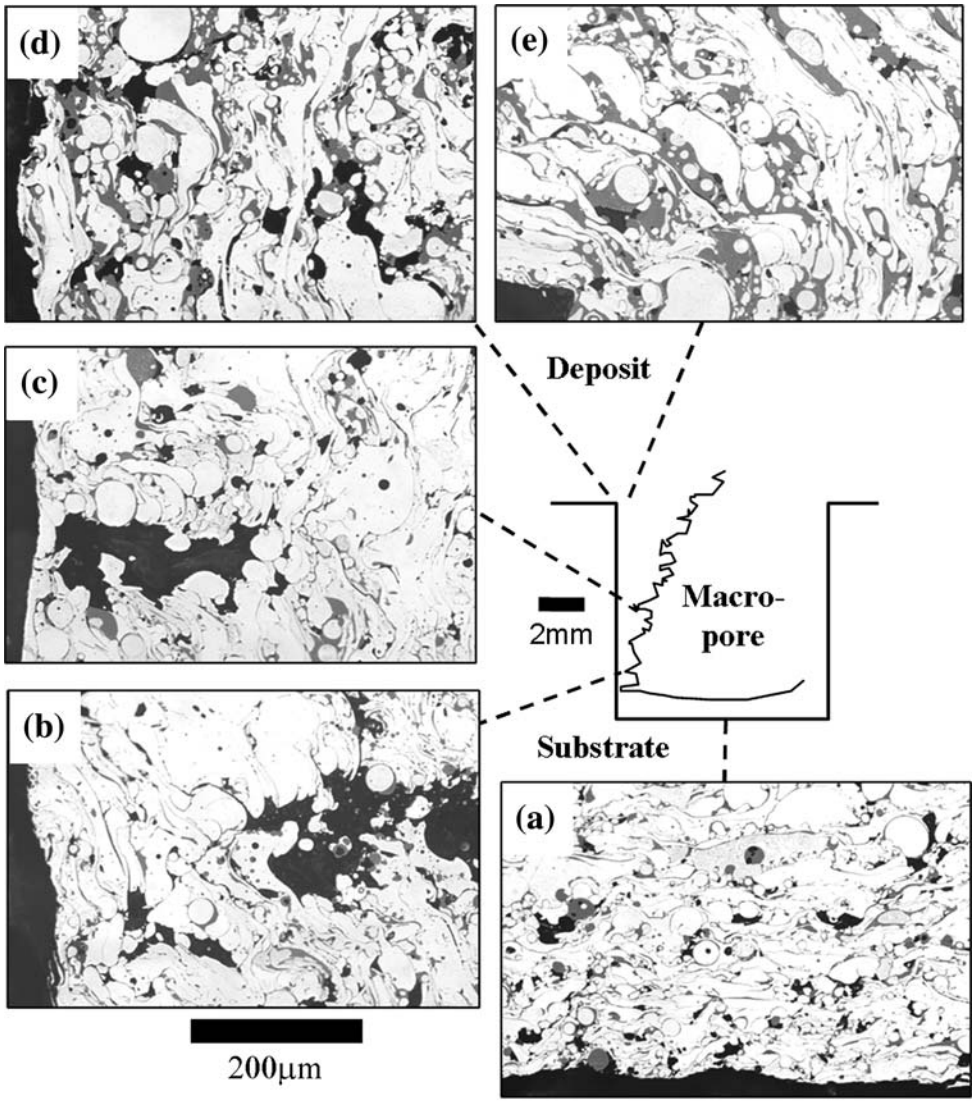

Fig. 11 Optical micrographs of different positions in a deposit formed by spraying into a 10 by 10 mm (standard) cylindrical hole, at an angle of 45° and an atomizing gas pressure of 140 kPa. (a) Hole base. (b) Side wall near base corner. (c) Side wall half-way up. (d) Side wall near top corner. (e) Top corner

porosity reduced to 5 to 10% approximately three-quarters of the way up. The side-wall oxide decreased from ~14 to ~9%, moving up from the base to half way. Both the amount of side-wall oxide and porosity increased near the top of the hole, as shown in Fig. 11(d), to ~18 and ~12%, respectively, Around the top corner, the amount of porosity was relatively low and the oxide was banded, with the oxide containing a high number of splash PSDs, as shown in Fig. 11(e).

3.4.3 Atomizing Gas Pressure. Increasing the atomizing gas pressure to 450 kPa, in common with the microstructure formed on the flat areas of the substrates, decreased the scale of the microstructure, that is, splat, pore, and PSD size, in and around the holes, and the oxide fractions significantly increased, as shown previously in Fig. 9 and 12, and subsequently in Fig. 14-17. Taking the 10 by 10 mm (standard) hole as an example, the oxide content of the side-wall deposits sprayed at 450 kPa exhibited the same trends moving away from the hole base, but with fractions that were double that of deposits sprayed at 140 kPa, as shown in Fig. 9(a) and 12(a). For the deposit sprayed at 450 kPa and 90°, high oxide fraction (and PSD) bands and coarser, relatively low oxide fraction bands from the top surface were interleaved and wrapped around the hole upper corner, as shown in Fig. 13. The effect of atomizing gas pressure on the side-wall porosity fraction was relatively small, as shown for the deposit sprayed at 45° in Fig. 12(b). For the specific case of the 10 by 10 mm hole sprayed at 90°, however, the deposit formed at a gas atomizing pressure of 450 kPa displayed a different trend to that sprayed at 140 kPa: the porosity increased to a maximum of ~22% at about two-thirds distance from the base, before decreasing to 13% at the top corner, as shown in Fig. 9(b).

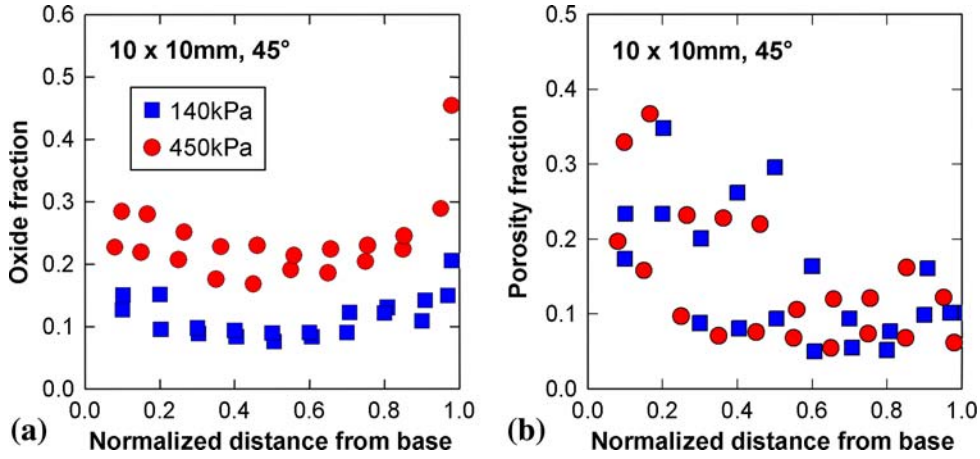

Fig. 12 Variation of (a) oxide and (b) porosity up the side walls of deposits formed by spraying into 10 by 10 mm (standard) cylindrical holes at an angle of 45° at atomizing gas pressures of 140 and 450 kPa

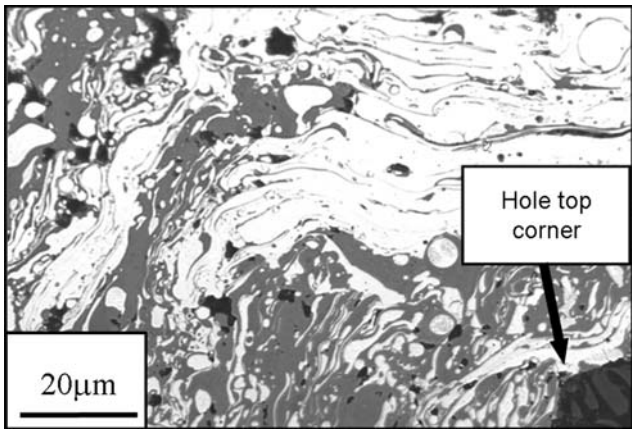

Fig. 13 Optical micrograph of the deposit around the top corner of a 10 by 10 mm cylindrical hole, sprayed at a angle of 90° and an atomizing gas pressure of 450 kPa

3.4.4 Constant Hole Aspect Ratio/Changing Dimensions. Increasing the hole size increased the amount of oxide, with the position of the maximum oxide fraction dependent on the spray angle. For the deposits sprayed at 90°, increasing the hole size accentuated the increase in the side-wall oxide with respect to distance from the hole base, as shown in Fig. 14(a) and (c). Taking the deposit sprayed at 450 kPa as an example, the side-wall oxide fraction in the 5 by 5 mm hole increased from ~18 to ~28% at the top corner, whereas for the 20 by 20 mm hole the equivalent values were ~22 and ~50%, respectively. For the deposits sprayed at 45°, increasing the hole size accentuated the minimum in the side-wall oxide with respect to distance from the hole base, as shown in Fig. 15(a) and (c). Again for 450 kPa, as an example, the side-wall oxide in the 5 by 5 mm hole decreased from ~23 to ~19%, before increasing to ~21% at the top corner, whereas for the 20 by 20 mm hole the equivalent values were ~36, ~21, and ~35%, respectively. The side-wall oxide fraction near the hole base for the 20 by 20 mm hole sprayed at 450 kPa and 45° was particularly variable, indicative of the banded microstructure described previously (Ref 17).

Increasing the hole size also increased side-wall porosity and changed the trend with respect to distance from the hole base. For the deposits sprayed at 90°, taking the deposit sprayed at 450 kPa as an example, the side-wall porosity in the 5 by 5 mm hole remained roughly constant at ~11%, before increasing to ~20% near the top corner, as shown in Fig. 14(b), displaying similar behavior to the 10 by 10 mm hole sprayed at 140 kPa (Fig 9b). In contrast, for the 20 by 20 mm hole, the side-wall porosity exhibited a wide (and variable) maximum, with porosity fraction increasing from ~16% to 9-32%, before decreasing to ~9% near the top corner, as shown in Fig. 14(d). For the deposits sprayed at 45°, the holes of different sizes displayed similar levels and trends of porosity as the 10 by 10 mm hole (Fig. 12b); that is, there was a maximum of 25 to 40% ~2 mm up the side wall, which then decreased to ~10% toward the top corner, as shown in Fig. 15(b) and (d). The high (and variable) fractions of porosity were again associated with the presence of large, linear pores fanning away from the side walls.

3.4.5 Constant Hole Diameter/Changing Aspect Ratio. The 10 by 15 mm (deep) holes sprayed with a gas atomizing pressure of 450 kPa were too fragile to enable a coherent deposit to be mounted, and oxide/porosity measurements could not be obtained, indicating the formation of deposit that was heavily oxidized, significantly porous, and/or too thin.

For the deposits sprayed at 90° (and at 140 kPa), the level and trend of side-wall oxide were similar, both increasing from ~10% near the base corner, with the 15 mm hole having a slightly greater amount of oxide of ~26%, compared with ~22% for the 5 mm hole, near to the top corner. The levels of side-wall porosity when sprayed at 90° were, however, very different, as shown in Fig. 16(b) and (d): whereas the 5 mm hole exhibited a relatively small variation in side-wall porosity fraction, in the range 9 to 17%, the 15 mm hole had a broad maximum of 39% halfway from the base. Likewise, for the deposits

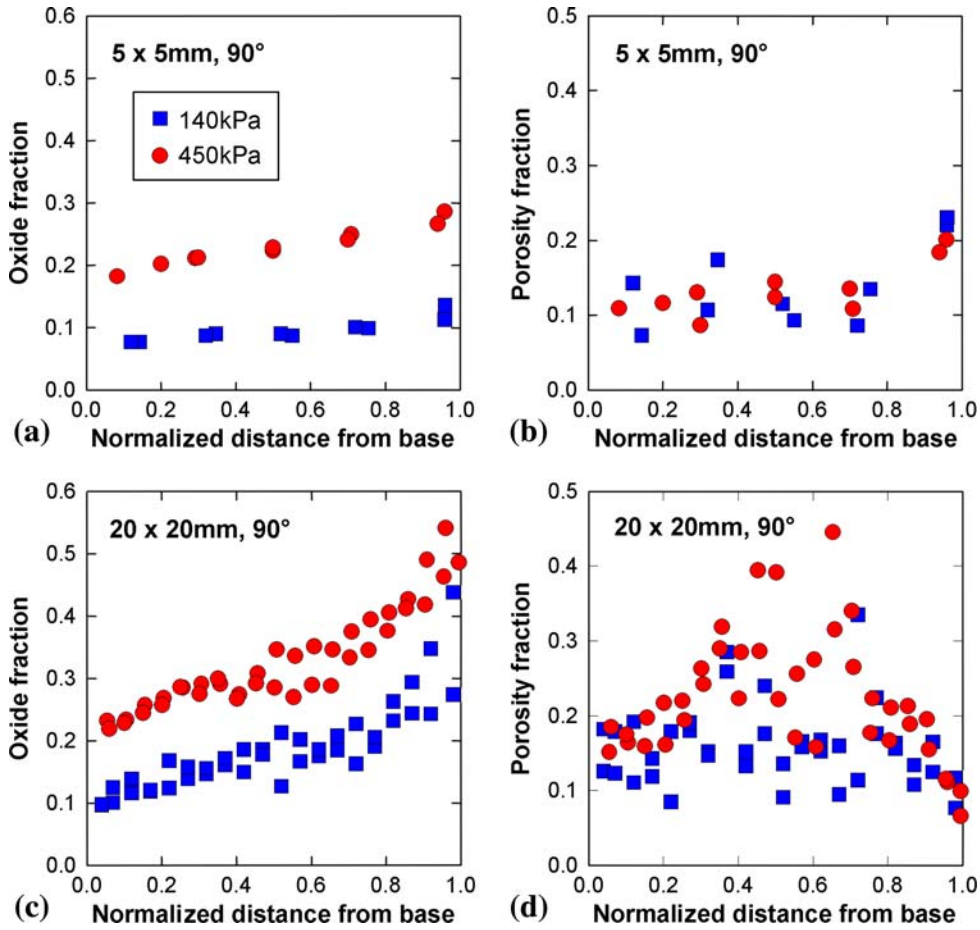

Fig. 14 Effect of hole size (at a constant 1:1 aspect ratio) on the variation of oxide and porosity up the side walls of deposits formed by spraying at an angle of 90°, and atomizing gas pressures of 140 and 450 kPa, into cylindrical holes. (a) and (b) 5 by 5 mm (small) and (c) and (d) 20 by 20 mm (large)

sprayed at 45° (and at 140 kPa), the fractions of side-wall oxide were similar, and the porosity very different, as shown in Fig. 17(b) and (d): the 5 mm hole exhibited a small decrease in porosity, from ~10 to ~6% at the top corner, and the 15 mm hole exhibited a strong maximum of ~70% at ~3 mm from the base, before decreasing to ~8% near the top corner.

The deposit formed on the centerline of the 10 by 5 mm (shallow) hole by spraying at 45° with an atomizing gas pressure of 450 kPa exhibited a varying microstructure caused by changes in the deposition mechanism as spraying proceeded and the deposit thickened. Near the base, the deposit contained a relatively low oxide and porosity, as shown in Fig. 18(a), similar to the deposit formed on flat areas of substrate. At a thickness of ~1.5 mm, the microstructure became finer, and the amount of oxide, porosity, and PSDs increased, as shown in Fig. 18(b). Most of this increase in porosity was caused by the presence of large, elongated pores, with their long axes perpendicular to the base. Near the surface of the teardrop-shaped macropore, these large pores were absent, as shown in Fig. 18(c). Overall, moving upward through the deposit from the base, the porosity exhibited a strong maximum, increasing from 6 to 30%, before decreasing to 13%, as shown in Fig. 18(d).

4. Discussion

4.1 Deposition of Splash Droplets

During the electric arc spraying of steel using N_2 atomizing gas, the entrainment of air into the primary spray results in oxidation of the molten steel droplets to form FeO (Ref 25). The oxide is incorporated into the deposit, primarily as thin, intersplat stringers as the droplets deposit. Turbulent intradroplet flow can lead to some of this oxide becoming mixed into the liquid interior to form a fine emulsion of spherical intrasplat oxide (Ref 25, 26). This is the dominant origin of oxide in thin coatings. When spraying thicker deposits, particularly trying to fill narrow substrate features, the amount of oxide can be greatly increased by the secondary deposition of splash droplets, because of their relatively small size, as shown in Fig. 5, and large surface area per unit volume. The relatively low velocity of splash droplets of 10 to 20 m/s compared with

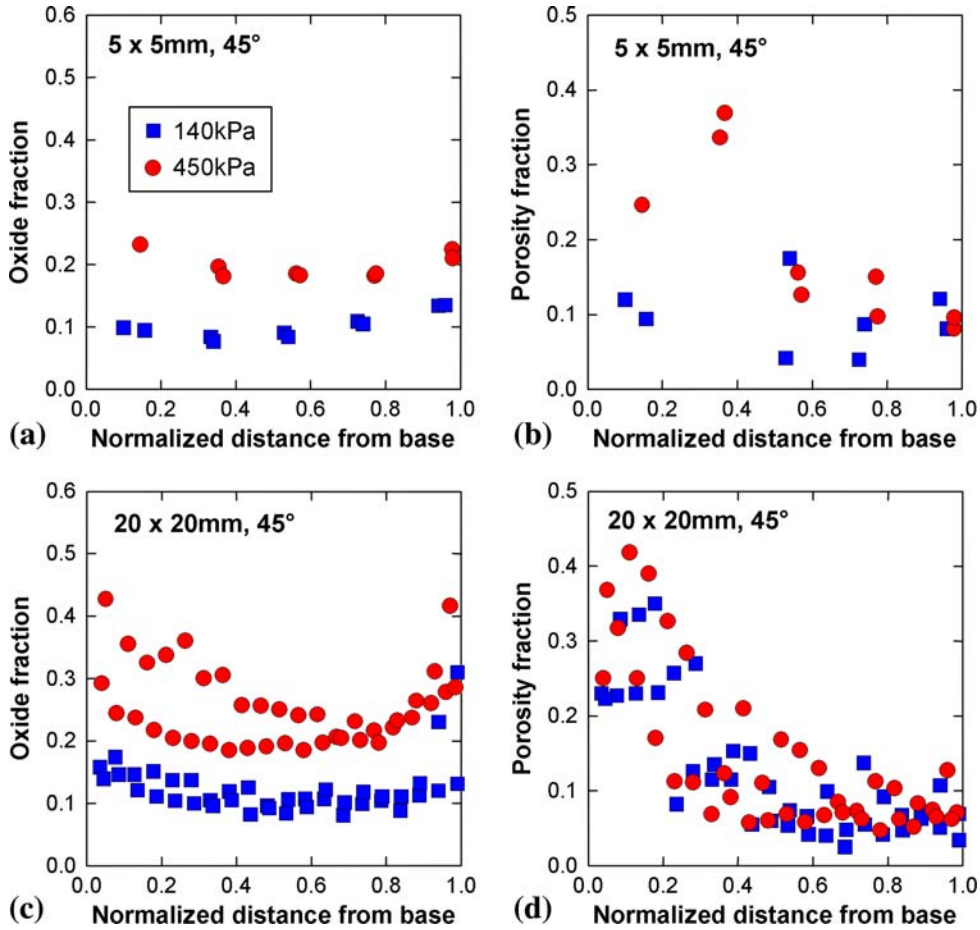

Fig. 15 Effect of hole size (at a constant 1:1 aspect ratio) on the variation of oxide and porosity up the side walls of deposits formed by spraying at an angle of 45°, and atomizing gas pressures of 140 and 450 kPa, into cylindrical holes. (a) and (b) 5 by 5 mm (small) and (c) and (d) 20 by 20 mm (large)

primary droplets of 50 to 70 m/s (Ref 17, 18) evidently provides sufficient time for oxidation reactions to occur, even over the relatively small flight distances.

Most of the splash droplets travel with trajectories close to the substrate/deposit top surface, as shown by Fig. 6 and previous observations (Ref 17, 18). As a result, deposition of splash droplets can occur when spraying onto substrates where no large topographical features exist initially, due to the presence of small perturbations on the substrate and/or coating, such as PSDs. Splash droplet deposition is increased for slower gun traverse speeds, when a significant step of material is present at the advancing front of the sprayed layer (Ref 27). Once a significant amount of splash material has deposited, the increased size of the perturbation acts to collect progressively more splash droplets, to create a diverging cone of high oxide material (Ref 25, 28), as shown in Fig. 7, a structural feature not usually observed in thin coatings.

4.2 Effect of Topography

The variation of oxide and porosity around pronounced topographical features can be explained by considering the relative proportions of primary (large diameter, high velocity, liquid, low oxidation) and splash (small diameter, low velocity, mushy or solid, highly oxidized) droplets depositing at a point and their angles of deposition. The parameters that determine the amount of oxide contributed by the splash droplets are their diameter and temperature; the time-of-flight, which controls the extent of solidification and oxidation; and the local oxygen partial pressure. When the atomizing gas pressure is increased, there is a significant decrease in primary and splash droplet diameters, as also shown by Fig. 5, increasing the amount of oxide significantly, as shown repeatedly in Fig. 9, 12, 14, and 17. If the splash droplets deposit relatively quickly, the steel is still molten and there is relatively little oxide. The characteristic microstructure, if shadowed from the primary spray, then predominantly comprises fine scale steel splats, with a relatively small amount of intersplat oxide. If the splash droplets deposit a longer time after formation, when the steel has solidified and is surrounded by significant liquid oxide, then the characteristic microstructure is an array of small steel PSDs in an oxide matrix. An increase in the hole diameter (at constant aspect ratio) increases the time-of-flight and

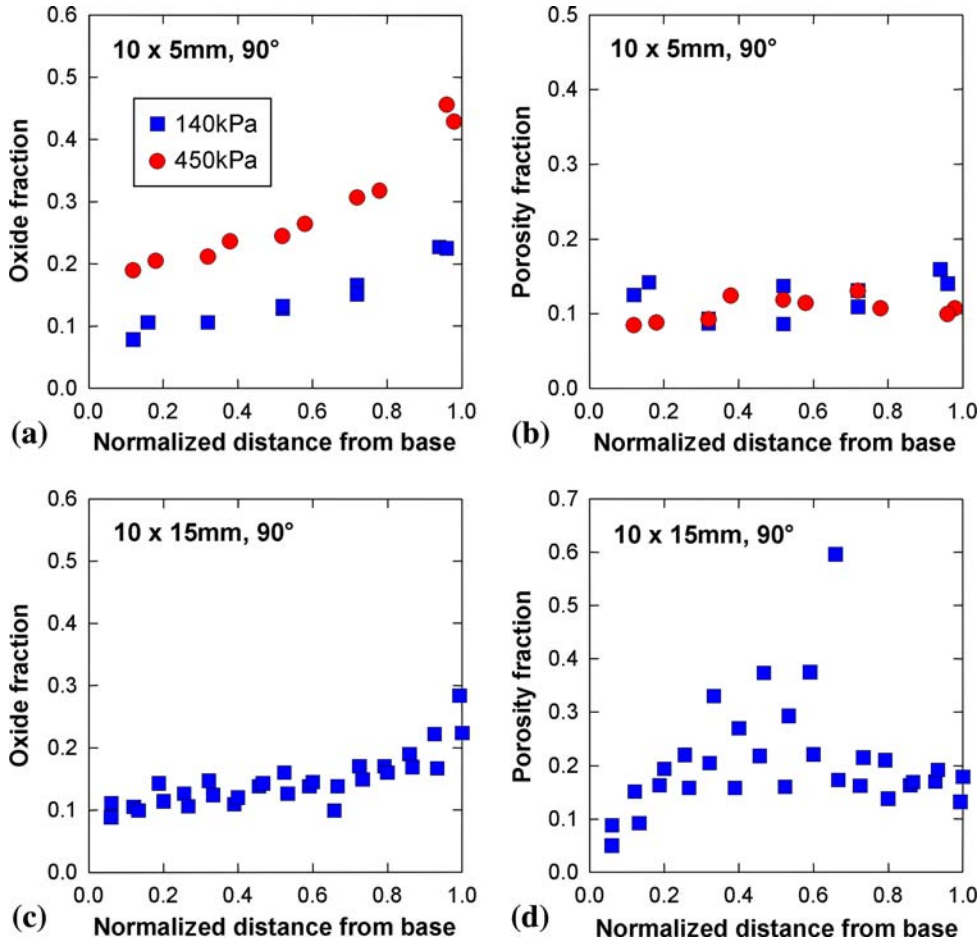

Fig. 16 Effect of hole depth (at a constant 10 mm diameter) on the variation of oxide and porosity up the side walls of deposits formed by spraying at 90°, at atomizing gas pressures of 140 and 450 kPa, into cylindrical holes. (a) and (b) 10 by 5 mm (shallow), and (c) and (d) 10 by 15 mm (deep)

leads to an increase in the oxide content of the side-wall deposit toward the top corner for that sprayed at 90°, and at both base and top corners for that sprayed at 45°, as shown in Fig. 14 and 15(a) and (c).

The porosity in regions of the deposit formed by highly oxidized splash droplets is influenced by the local temperature and the extent of oxide flow, just as the flow of steel droplets determines porosity in the deposit formed from the primary spray. However, the angle of deposition, for both the primary spray and the splash droplets, can be more important in determining porosity; an acute angle leads to large, linear pores and extremely high (and variable) local porosity levels, particularly noticeable for larger and deeper holes, as shown in (d) in Fig. 14-17.

Figure 19 shows schematically how splash droplets may deposit when spraying in and around a cylindrical hole of 1:1 aspect ratio, in an otherwise flat substrate. At a spray angle of 90° to the substrate top surface, when the spray axis is coincident with the hole, Fig. 19(a), splash droplets deposit on the side walls of the hole, forming deposit such as that shown in Fig. 8(b). When the primary spray axis intersects the substrate top surface near the hole, Fig. 19(b), a significant flux of splash droplets is incident on the opposite wall very near the top corner, as shown in Fig. 6 and previous work (Ref 18), forming a deposit here such as that shown in Fig. 8(d) and (e). At a spray angle of 45°, when the spray axis is within the hole, Fig. 19(c), the primary spray impacts the side walls of the hole and deposition of splash droplets occurs on the base, forming deposit such as that shown in Fig. 11(a). When the 45° primary spray axis intersects the substrate top surface near the hole, Fig. 19(d), deposition of splash droplets occurs on the opposite side wall, near the top corner, in addition to the deposition of the primary spray, forming deposit such as that shown in Fig. 11(d) and (e).

4.3 Bridging and Macropore Formation

4.3.1 Spray Angle of 90°. When spraying into a hole at an angle of 90°, such as those studied here, the side walls are largely shadowed from the primary spray, but bridging can still occur and may be explained with reference to the sequence of schematic diagrams in Fig. 20:

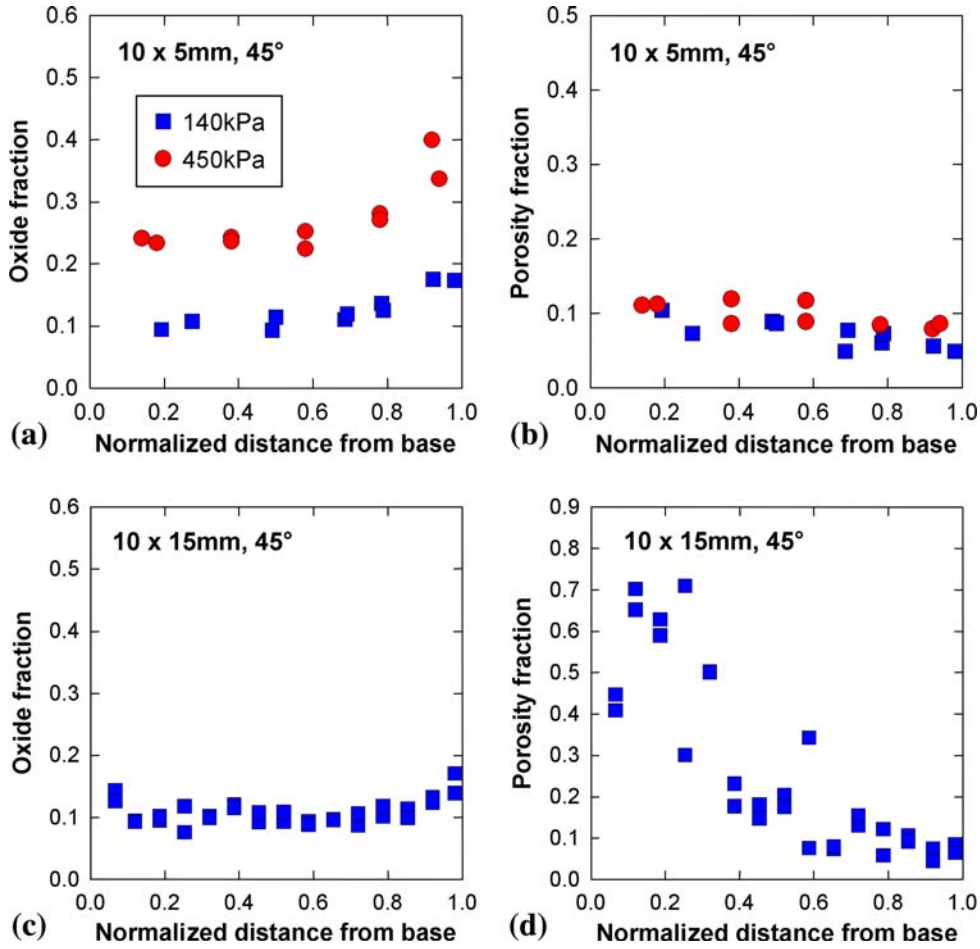

Fig. 17 Effect of hole depth (at a constant 10 mm diameter) on the variation of oxide and porosity up the side walls of deposits formed by spraying at 45°, at atomizing gas pressures of 140 and 450 kPa, into cylindrical holes. (a) and (b) 10 by 5 mm (shallow), and (c) and (d) 10 by 15 mm (deep)

Stage I. Oxidized splash droplets, from the opposite corner of the hole, deposit around the top corner, forming a high oxide, porosity, and PSD-containing deposit that on average grows toward the spray source, that is, across the hole.

Stage II. Primary droplets impinge on the splashed material, and the deposit grows toward the spray source, that is, the gun.

Stage III. The overhang of deposit grows in a direction that is the result of the continuing primary and secondary deposition and their associated growth directions, eventually reaching the hole axis, when the bridge is complete and a macropore is formed.

Thus, the microstructure around the top corner of the hole consists of interweaved bands of large splats and PSDs in an oxide matrix, most clearly shown in Fig. 13. The inverse heart-shaped macropore arises as a result of progressive shadowing of the base as bridging occurs. Although splashing of droplets on the base leads to deposit formation on the side wall near the base corner, bridging restricts the amount of splash deposition near the top corner, typically leading to a thin deposit at this point, consisting mostly of more highly oxidized splash droplets from the opposite top corner.

4.3.2 Spray Angle of 45°. Rapid bridging occurs at a spray angle of 45° because primary deposition on the top corners automatically leads to deposit growth direction with a component across the hole (Ref 20). The addition of splash droplets increases bridging speed and leads to a structure consisting of continuous, alternating bands of steel splats and finer, highly oxidized, high PSD-containing material, as shown in Fig. 11(e).

A consequence of bridging when spraying onto a substrate containing a hole of 1:1 aspect ratio at an angle of 45° is that the deposit on the side walls is very thin near the base corner. At the start of spraying, all of the side wall is visible to the spray. As the deposit begins to grow on the top surface and top corner, the lower side wall quickly becomes shadowed, the shadow moving progressively upward. Any deposit that then forms in these shadowed regions can only arise from the deposition of splash droplets generated from nonshadowed regions further up (Ref 17). This deposition occurs at an acute angle, leading

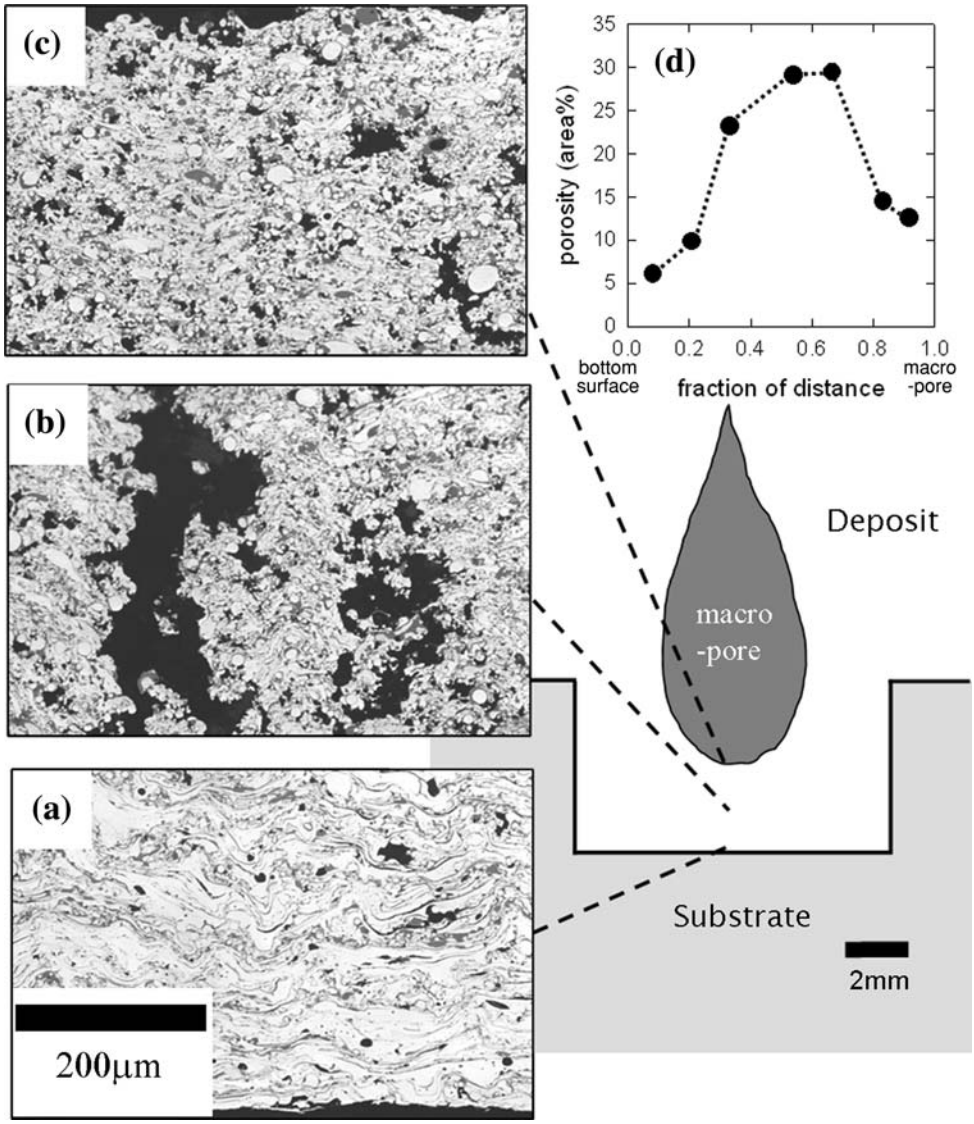

Fig. 18 Optical micrographs showing the variation in microstructure on the hole axis of a deposit formed by spraying into a 10 by 5 mm (shallow) hole at an angle of 45° with an atomizing gas pressure of 450 kPa. (a) Base. (b) Halfway between the base and the macropore. (c) At the macropore surface. (d) Graphical variation of deposit porosity between the base and the macropore

to the formation of large, linear pores, as shown in Fig. 11(b) and (c). Thus, not only is the deposit near the base corner thin, it is oxidized and highly porous. Further up the side wall, both oxide and porosity decrease because of a greater contribution of the primary spray. The oxide then increases near the top corner as a result of the deposition of splash droplets originating from the opposite corner.

4.4 Transient Effects

As spraying proceeds, the aspect ratio of a hole, the ratio of depth to diameter, can effectively increase, since material can build up on the sides without sufficient spray depositing on the base. Consequently, there can be a change in the active deposition mechanism on a particular part of the substrate. For example, consider the 10 by 5 mm hole sprayed at an angle of 45°, for which the axial deposit microstructure was shown in Fig. 18. In stage I, at the start, the base of the hole is visible to the primary spray, leading to a microstructure with relatively low oxide and porosity. However, growth of the deposit at the top corners leads to progressive shadowing of the base. In stage II, when the base becomes shadowed, growth continues by the deposition of splash droplets originating from the side walls that have remained visible to the primary spray. As a result of the acute angle of deposition, alternating from side to side, large, linear pores are formed. The amount of oxide also increases. In stage III, a short time before closure of the macropore, only the deposit at the tips of the bridge is visible. Splash droplets still enter the hole and deposit on the base at an angle close to 90°. Although the amount of oxide

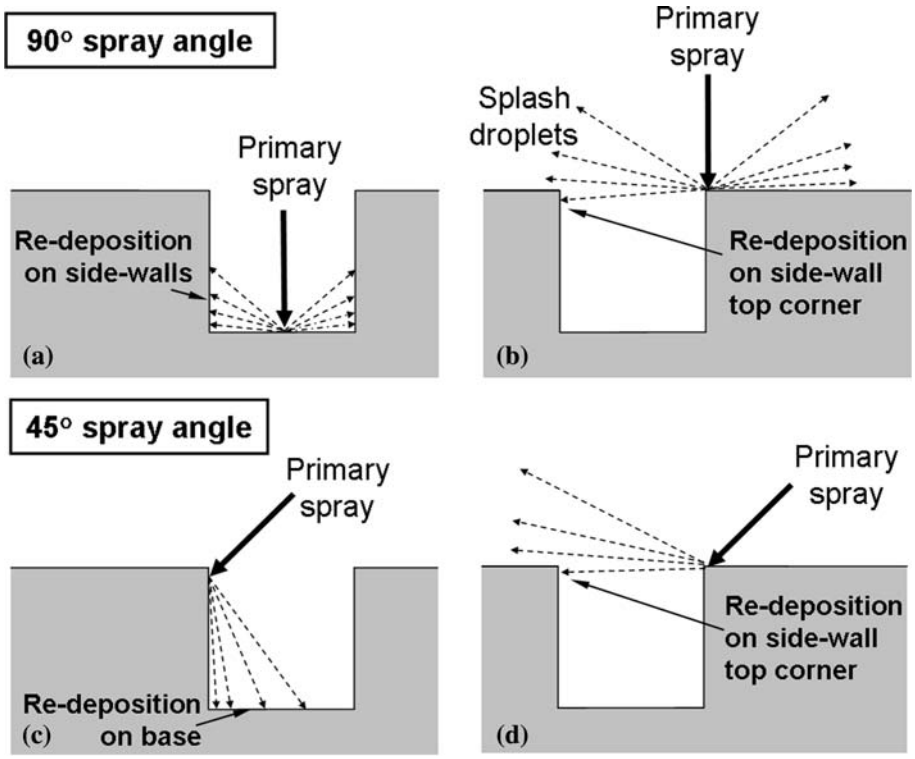

Fig. 19 Schematic diagram showing how splashing as the spray traverses leads to secondary deposition of splash droplets onto a substrate containing a hole. Spray angle of 90°: (a) spray axis on hole axis and (b) spray axis on top surface near corner. Spray angle of 45°: (c) spray axis on hole axis and (d) spray axis on top surface near corner

remains high, the near-normal deposition reduces the porosity.

4.5 Implications for the Manufacture of Spray Formed Tooling

Electric arc spray forming has successfully made robust, dimensionally accurate steel tools, up to 0.8 by 0.6 m, which have manufactured many thousands of parts (Ref 6, 15). In order to realize the potential for spray formed tools of progressively larger size and complexity, plus improving the tool performance and decreasing the requirement for postspray machining, a number of changes to the initial spraying parameter can be made. From the observations made in this study, the most important of these are:

Spray angle. Spraying at 90° ensures good quality material in the base of narrow features, but it can lead to the formation of poor quality material on the side walls near the top, particularly if a large amount of oxidation occurs and bridging prevents sufficient filling. Spraying at 45° improves the side-wall deposit at the top, but leads to poor side-wall material near the base and further exacerbates the problem of bridging. An intermediate spray angle could be optimal, and indeed, current industrial best practice employs a single 90° gun with three, radially distributed, 45° guns (Ref 15). However, it is considered that as long as the primary spray remains directed at the base of the feature and oxidation can be limited (so that bridging is minimized and high-quality splash deposit can be formed on shadowed surfaces), an angle close to 90° is preferred.

Atmosphere. Improved shrouding or atmosphere control within the spray booth, particularly near the substrate to reduce the local oxygen concentration, would lead to a lower spray temperature (Ref 24) and decrease the amount of oxide incorporated in the deposit. It would also have the benefit of reducing carbon loss in the steel (Ref 25), leading to a harder tool surface.

Robotic path planning. Approaches that allow robot path, gun angle, and spray strategies to be chosen on the basis of the specific topography of the substrate and the way in which topography evolves as deposition proceeds must be developed. In practice, this requires reprogramming of the robot path ''on-the-fly'' and is far from trivial. Further, complex robot paths tend to lead to low robot velocities and other problems (Ref 15). For small-diameter holes, a near-stationary gun to keep the primary spray axis remaining on the base would also be problematic with respect to an excess deposit temperature and thickness. For a channel, the spray axis should be moved along the long direction, rather than traversing across it.

Droplet size. By using a low atomizing gas pressure, the amount of oxide in the deposit can be substantially

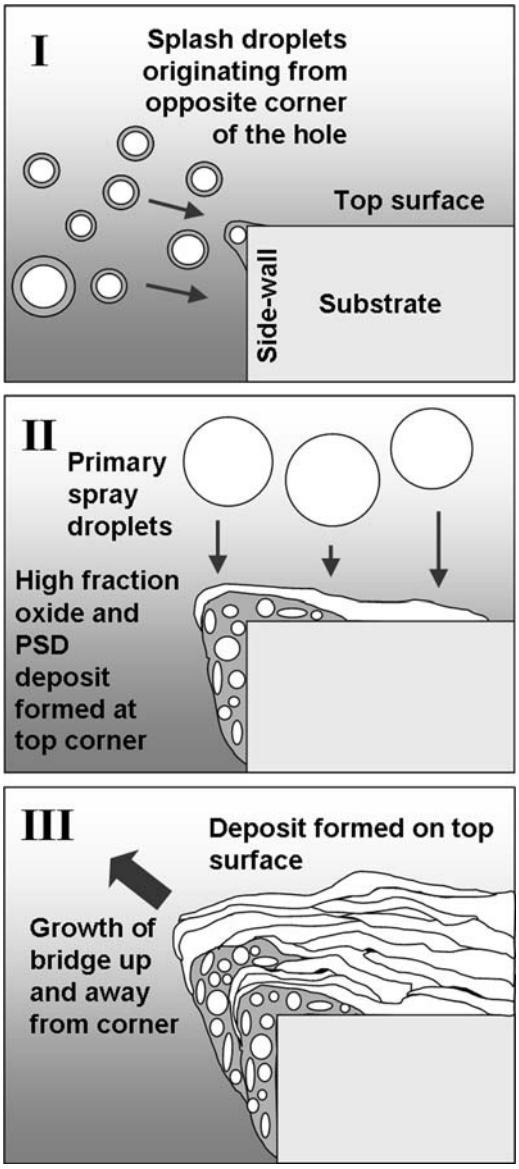

Fig. 20 Sequence of schematic diagrams showing how the combined secondary deposition of splash droplets (originating from the opposite side of the hole) and the primary spray leads to bridging across a hole when spraying at an angle of 90°

reduced because of an increase in the splash droplet diameter. With a droplet diameter larger than used here, the effects of bridging and shadowing can be reduced, and the ability to reproduce edges and corners improved (Ref 29).

5. Conclusions

Droplet splashing at deposition during the electric arc spraying of Fe-0.8 wt.%C steel has been shown to play a critical role in determining the microstructure of thick deposits. Secondary deposition of splash droplets leads to pronounced interpass bands and vertical columns of high oxide for a deposit formed on an initially flat substrate. For the spraying of substrates with significant topography, spray angle, atomizing gas pressure, and feature shape and size have been shown to be influential in determining deposit structure. The local oxide and porosity depends on the relative proportions of primary and secondary droplets depositing at a point and on their angles of deposition. Increases in atomizing gas pressure lead to finer microstructures and to an increase in oxide fraction because of the promotion of smaller-diameter primary and splash droplets. Splash droplets can be beneficial in forming a deposit on surfaces shadowed from the primary spray. However, splash droplet deposition, combined with primary deposition, leads to increased bridging and the formation of macropores. Spraying at 45° may increase the amount of deposit on the side walls of substrate holes, particularly near the top corner, but increases the problem of bridging. The filling of severe substrate features can be improved, and the potential for spray formed tooling enhanced, by manipulating the spray so that it is perpendicular to the general substrate surface and remains as close as possible to the feature axis prior to the completion of filling. Thus, robot path planning must be implemented to account for specific substrate topography, particularly during the initial stage of spraying. Additionally, using a low atomizing gas pressure and reducing the oxygen concentration in the atmosphere surrounding the spray would be beneficial.

Acknowledgment

The authors would like to thank Allen Roche and Jon Betts for their assistance with robotic spraying and freeze casting of the ceramic substrates.

References

1. D.E. Crawmer, Thermal Spray Processes, *Handbook of Thermal Spray Technology,* J.R Davis, Ed., ASM International, 2004, p 54-76
2. B. Cantor, K-H. Baik, and P.S Grant, Development of Microstructure in Spray Formed Alloys, *Prog. Mater. Sci.*, 1997, **42**, p 373-392
3. M.M. Fasching, F.B Prinz, and L.E. Weiss, Planning Robotic Trajectories for Thermal Spray Shape Deposition, *J. Thermal Spray Technol.*, 1993, **2**, p 45-57
4. L.E. Weiss, E.L. Gursoz, F.B. Prinz, P.S. Fussell, S. Mahalingam, E.P. Patrick, and A Rapid, Tool Manufacturing System Based on Stereolithography and Thermal Spraying, *Manuf. Rev.*, 1990, **3**, p 40-48
5. P.S. Fussell, H.O.K. Kirchner, F.B. Prinz, and L.E. Weiss, Controlled Microstructure of Arc Sprayed Metal Shells, *J. Thermal Spray Technol.*, 1994, **3**, p 148-161
6. A.P. Newbery, P.S. Grant, R.M. Jordan, A.D. Roche, and T. Carr, The Electric Arc Spray Manufacture of Rapid Production Tooling, *Thermal Spray: Meeting the Challenges of the 21st Century,* C. Coddet, Ed., May 25-29, 1998 (Nice, France), ASM International, 1998, p 1223-1228
7. C.K. Chua, K.H. Hong, and S.L. Ho, Rapid Tooling Technology. Part 2. A Case Study Using Arc Spray Metal Tooling, *Int. J. Adv. Manuf. Technol.*, 1999, **15**, p 609-614

8. H.M. Hu, E.J. Lavernia, Z.H. Lee, and D.R. White, Residual Stresses in Spray Formed A2 Tool Steel, *J. Mater. Res.*, 1999, **14**, p 4521-4530
9. D.I. Wimpenny and G.J. Gibbons, Metal Spray Invar Tooling for Composites, *Aircraft Eng. Aerospace Technol.*, 2000, **72**, p 430-439
10. H.M. Hu, Z.H. Lee, D.R. White, and E.J. Lavernia, On the Evolution of Porosity in Spray Deposited Tool Steels, *Met. Mater. Trans. A*, 2000, **31**, p 723-733
11. H. Zhang, G. Wang, Y. Luo, and T. Nakaga, Rapid Hard Tooling by Plasma Spraying for Injection Molding and Sheet Metal Forming, *Thin Solid Films*, 2001, **390**, p 7-12
12. I.K. Hui, M. Hua, and H.C.W. Lau, A Parametric Investigation of Arc Spraying Process for Rapid Mould Making, *Int. J. Adv. Manufact. Technol.*, 2003, **22**, p 786-795
13. P.D.A Jones, S.R. Duncan, T. Rayment, and P.S. Grant, Control of Temperature Profile for a Spray Deposition Process, *IEEE Trans. Control Sys. Tech.*, 2003, **11**, p 656-667
14. S. Hoile, T. Rayment, and P.S. Grant, Phase Transformations and Control of Residual Stresses in Thick Spray Formed Steel Shells, *Met. Mater. Trans. B*, 2004, **35**, p 1113-1122
15. A. Roche, S.R. Duncan, and P.S. Grant, Scientific Technological and Economic Aspects of Rapid Tooling by Electric Arc Spray Forming, *J. Thermal Spray Technol.*, 2006, **15**, p 796-801
16. M.P. Kanouff, R.A. Neiser, and T.J. Roemer, Surface Roughness of Thermal Spray Coatings Made with Off-Normal Spray Angles, *J. Thermal Spray Technol.*, 1998, **7**, p 219-228
17. A.P. Newbery and P.S. Grant, Droplet Splashing During Arc Spraying of Steel and the Effect on Deposit Microstructure, *J. Thermal Spray Technol.*, 2000, **9**, p 250-258
18. A.P. Newbery, T. Rayment, and P.S. Grant, A Particle Image Velocimetry Investigation of In-Flight and Deposition Behaviour of Steel Droplets During Electric Arc Sprayforming, *Mater. Sci. Eng. A*, 2004, **383**, p 137-145
19. Z. Djuric, P. Newbery, and P. Grant, Two-Dimensional Simulation of Liquid Metal Spray Deposition onto a Complex Surface, *Modell. Sim. Mater. Sci. Eng.*, 1999, **7**, p 553-571
20. Z. Djuric and P.S. Grant, Two-Dimensional Simulation of Liquid Metal Spray Deposition onto a Complex Surface II: Splashing and Redeposition, *Modell. Sim. Mater. Sci. Eng.*, 2001, **9**, p 111-127
21. J. Mi and P.S. Grant, Modelling the Shape and Thermal Dynamics During the Spray Forming of Ni Superalloy Rings Part 1: Droplet Deposition, Splashing and Re-Deposition, *Acta Mater.*, 2008, **56**, p 1588-1596
22. J. Mi and P.S. Grant, Modelling the Shape and Thermal Dynamics During the Spray Forming of Ni Superalloy Rings. Part 2: Heat Flow and Solidification, *Acta Mater.*, 2008, **56**, p 1597-1608
23. A.P. Newbery and P.S. Grant, Large Voltage Fluctuations and Droplet Formation in Electric Arc Wire Spraying, *Powder Metall.*, 2003, **46**, p 229-235
24. A.P. Newbery, P.S. Grant, and R.A. Neiser, The Velocity and Temperature of Steel Droplets During Electric Arc Spraying, *Surf. Coat. Technol.*, 2005, **195**, p 91-101
25. A.P. Newbery and P.S. Grant, Oxidation During Electric Arc Spray Forming of Steel, *J. Mater. Proc. Technol.*, 2006, **178**, p 259-269
26. R.A. Neiser, M.F. Smith, and R.C. Dykhuizen, Oxidation in Wire HVOF-Sprayed Steel, *J. Thermal Spray Technol.*, 1998, **7**, p 537-545
27. M.K. Hedges, A.P. Newbery, and P.S. Grant, Characterisation of Electric Arc Spray Formed Ni Superalloy IN718, *Mater. Sci. Eng. A*, 2002, **326**, p 79-91
28. S. Hoile, T. Rayment, P.S. Grant, and A. Roche, Oxide Formation in the Sprayform Tool Process, *Mater. Sci. Eng. A*, 2004, **383**, p 50-57
29. R.M. Jordan, J. Betts, P. Grant, A. Roche, and P. Newbery, Spray Deposition Process, U.S. Patent No. 6,623,808, 2003